

Tides of the Ross Sea and Ross Ice Shelf cavity

LAURENCE PADMAN^{1*}, SVETLANA EROFEEVA² and IAN JOUGHIN³

¹Earth & Space Research, 1910 Fairview Ave E, Suite 102, Seattle, WA 98102-3620, USA

²College of Oceanic & Atmospheric Sciences, Oregon State University, Ocean Administration Building 104, Corvallis, OR 97331-1503, USA

³Jet Propulsion Laboratory, Mail Stop 300-235, 4800 Oak Grove Drive, Pasadena, CA 91109, USA

*address for correspondence: Earth & Space Research, 3350 SW Cascade Ave, Corvallis, OR 97333-1536, USA
padman@esr.org

Abstract: Two new ocean tide models for the Ross Sea which include the ocean cavity under the Ross Ice Shelf, are described. The optimum model for predicting ice shelf surface height variability is based on assimilation of gravimetry-derived tidal constituents from the Ross Ice Shelf. Synthetic aperture radar interferograms provide an independent test of model performance. The standard deviation of tide height variability is largest under the eastern ice shelf along the Shirase and Siple Coasts, where it can exceed 0.8 m. The maximum peak-to-peak tidal range in this region is ~3 m. The best predictor for ocean tidal currents north of the ice front is a dynamics-based model that solves the depth-integrated shallow water equations with a linear representation of benthic friction rather than the more usual quadratic form. Tidal currents over the open Ross Sea are dominated by diurnal, topographically trapped vorticity waves. The strongest modelled currents exceed 1 m s⁻¹ at spring tide in a narrow band along the upper continental slope in the north-western Ross Sea. Typical tidal currents in the central continental shelf area of the Ross Sea are 10–20 cm s⁻¹. Under the ice shelf the typical currents are ~5 cm s⁻¹.

Received 15 February 2002, accepted 6 September 2002

Key words: altimetry, data assimilation, ice shelves, inverse modelling, mixing, synthetic aperture radar

Introduction

The ocean tide is a major contributor to the variability of sea surface height (SSH) and currents throughout the world ocean, including the seas surrounding Antarctica. Previous attempts to characterize the distribution of tidal SSH and currents in the Ross Sea include analyses of gravimeter measurements on the Ross Ice Shelf (Williams & Robinson 1980) and numerical simulations by MacAyeal (1984, hereinafter denoted M84). Recent global models, such as the Finite Element Simulation (FES) (le Provost *et al.* 1998, Lefèvre *et al.* 2002) and TPXO.5 (G. Egbert, personal communication 2002), improve the description of tides in the Ross Sea. The Circum-Antarctic Tidal Simulation (CATS) model (Padman *et al.* 2002) further improves the quality of tidal simulation around Antarctica by using smaller grid spacing, and paying more attention to the accuracy of the grid geometry, than do the global models. None of these models, however, are able to represent the SSH and current measurements with sufficient accuracy for modern applications.

The principal limitations on tide model skill around Antarctica are as follows. First, the TOPEX/Poseidon satellite radar altimetry data set, which is the primary data constraint in recent data-assimilation global tidal models, does not extend poleward of ~66°. This latitude is well north of the major Antarctic embayments of the Ross and Weddell seas. Second, tide models that rely on dynamics rather than simply describing data are ultimately dependent

upon the quality of the model depth grid. Bathymetric data are sparse throughout most of the Southern Ocean. Under the large floating ice shelves, we also need to know the location of the grounding line and the distribution of water column thickness (the vertical separation between the ice base and the seabed). While recent satellite data allow us to accurately map grounding lines in many areas (e.g. Gray *et al.* 2002), for the Ross Ice Shelf (RIS) we still rely on coarsely spaced water column thickness measurements reported by Greischar & Bentley (1980).

We use a combination of dynamical modelling and data assimilation to develop a more accurate tide model for the Ross Sea. In this paper we review the available tidal SSH and velocity data in the Ross Sea, briefly describe the dynamical and data assimilation models, and describe the output and performance of the new models.

Tidal measurements in the Ross Sea

Sea Surface Height

The locations of sites for which we have tidal SSH coefficients (Fig. 1, Table I) are as reported by Williams & Robinson (1980). The original data consist of gravimeter records for periods of 30–58 days at nine sites on the RIS, plus a year-long tide gauge record at the McMurdo station. The gravity signals were converted to heights, corrected for the contribution from the solid earth tide, and then analysed

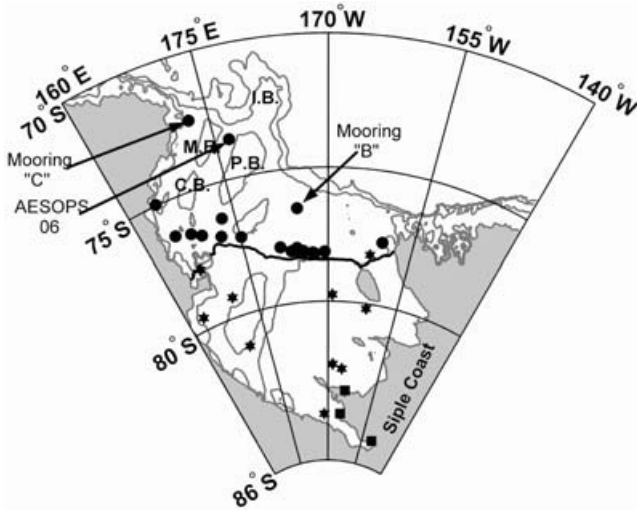


Fig. 1. Locations of major geographical features in the Ross Sea, including: I.B. = Iselin Bank, M.B. = Mawson Bank, C.B. = Cray Bank, P.B. = Pennell Bank. Depth contours (water column thickness under the Ross Ice Shelf) are shown for the 400, 1000 and 2000 m isobaths. Asterisks indicate locations of tide gauge data (see Table I). Solid squares show the three locations where six independent estimates of height change (δh) were obtained from SAR interferograms. Solid circles indicate locations of currents meters used in this study (see Table II).

for amplitudes and phases of six constituents. When comparing these data to models we make the assumption that, beyond some flexural boundary layer, the shelf ice is floating freely on the ocean surface. This is a reasonable assumption for sites more than a few kilometres seaward of the grounding line (Rignot *et al.* 2000).

Ice shelf surface height variability is also measured with Interferometric Synthetic Aperture Radar (InSAR). With sufficient InSAR imagery for a single region, several tidal constituents could be derived from the data (Rignot *et al.* 2000, appendix B). In practice, however, the limited number of available SAR interferograms at this time precludes this approach. For the present study, InSAR data were used to estimate the change in ice shelf surface height δh between time-separated satellite passes, to provide a small independent data set for comparing the relative skill of the various tide models considered herein. A total of six independent values of δh were obtained at three locations (Fig. 1), with 24 days separating the two SAR scenes in each InSAR pair. These measurements were obtained by examining profiles of the interferometric phase across grounding lines. After removing the effect of topography, the phase is proportional to displacement in the radar-line-of-sight from one pass to the next. The profiles were chosen in areas where there was little horizontal motion (e.g. relatively stagnant ice in sheltered embayments) or there was a smooth regular gradient in velocity that could easily be detrended. Areas such as across shear margins where there was a horizontal motion that could be easily confused

Table I. Location of tide height data on the Ross Ice Shelf (RIS), after Williams & Robinson (1980). All measurements were made with gravimeters mounted on the RIS, with the exception of the bottom pressure gauge record at McMurdo. Measurements are ordered roughly clockwise around the perimeter of the RIS from the eastern end of the ice front (LAS) to the western end (McMurdo).

Station	Location	Duration (days)
LAS	78.20°S, 162.27°W	32
C36	79.75°S, 169.05°W	34
RI	80.19°S, 161.56°W	36
Base	82.53°S, 166.00°W	44
J9	82.37°S, 168.63°W	30
F9	84.25°S, 171.33°W	58
C16	81.19°S, 170.50°E	45
O19	79.53°S, 163.36°E	39
C13	79.25°S, 170.37°E	34
McMurdo	77.85°S, 166.66°E	365

with tidal displacement were avoided. At each location, at least three profiles were selected that exhibited a clear and consistent displacement signal across the flexure zone. The differences in phase from the firmly grounded ice relative to the floating ice were then converted to relative vertical displacements. The largest source of error is due to incorrect mapping of horizontal displacements into vertical

Table II. Locations of selected Ross Sea current meters used in model validation studies. Selection criteria are explained in the velocity section.

Identifier ¹	Location	Meter depth (m)	Water depth (m)
PRISM 461	78.227°S, 172.490°W	383	420
PRISM 462	78.183°S, 174.650°W	237	530
PRISM 466	74.965°S, 164.393°E	780	879
PRISM 467	77.680°S, 160.403°W	255	590
PRISM 470	78.163°S, 170.612°W	305	558
PRISM 475	78.108°S, 174.513°W	285	567
PRISM 476	77.978°S, 175.597°W	210	585
PRISM 480	78.098°S, 175.503°W	225	558
PRISM 483	78.078°S, 176.658°W	425	595
PRISM 484	77.882°S, 178.533°W	340	700
PRISM 488	77.207°S, 175.155°E	350	685
PRISM 492	78.192°S, 172.800°W	240	436
R 001	76.706°S, 169.022°E	42	818
R 003	76.340°S, 165.054°E	212	815
R 005	76.982°S, 171.979°E	210	660
R 007	76.339°S, 172.937°E	196	669
J Mooring A	76.502°S, 167.500°E	241	775
J Mooring B	76.497°S, 174.993°W	241	569
J Mooring C	72.480°S, 172.525°E	241	533
AESOPS 06	73.543°S, 176.886°E	225	565

¹ Identifiers:

PRISM = see Pillsbury & Jacobs (1985). Data courtesy of D. Pillsbury. The number refers to the Accession Number of the current meter in the Oregon State University current meter database.

R = Research on Ocean-Atmosphere Variability and Ecosystem Response in the Ross Sea (ROAVERRS). Data courtesy of M. Van Woert.

J = See Jaeger *et al.* (1996). Data courtesy of J. Nittrouer.

AESOPS: Antarctic Environment Southern Ocean Process Study. Data courtesy of R. Collier.

displacements. We limited analyses to regions where these errors were less than ~ 10 cm.

Velocity

Current meter moorings have been deployed in the Ross Sea for several projects, starting with PRISM in the early 1980s (Pillsbury & Jacobs 1985). Several current meter records (Fig. 1, Table II) were selected to help validate our numerical models, focusing on meters that are well above the seabed and well below the surface layer. Tidal analysis of each of these records was performed using a Matlab™ tidal analysis software package that was kindly provided by R. Pawlowicz. This software (Pawlowicz *et al.* 2002) is a version of the Foreman (1977, 1978) FORTRAN-based tidal analysis package.

Tidal models

The discussion of modelling methods here is restricted to the essential features required to interpret the model results. We use “forward” (dynamical) and “inverse” (data assimilation) models, as described below.

Forward model

The two forward models are recent versions of CATS, which solves the depth-integrated shallow water equations as presented by Robertson *et al.* (1998). The CATS domain is the entire ocean south of 58°S including the ocean cavity under the ice shelves. The grid spacing is $1/4^\circ \times 1/12^\circ$, which gives ~ 10 km resolution near the Antarctic coast. The two models differ in their parameterization of bottom friction - CATS01.02 uses a standard quadratic representation while CATS02.01 uses linear friction. Quadratic friction is usually regarded as more realistic; however, the linear friction model performs significantly better in comparisons with both height and current data from the Ross Sea. Both models are forced by known astronomical forcing and specified elevation along the open ocean northern boundary at 58°S . This boundary condition is obtained from the quasi-global tidal model, TPXO.5, which is an updated version of the TPXO.3 model reported by Egbert (1997). The TPXO.5 model is constrained by assimilation of TOPEX/Poseidon (T/P) radar altimetry data. Ten tidal harmonics are modelled (see Table III). Predictions are made from this set of harmonics by introducing additional harmonics that modulate the tidal energy through the course of the

~ 18.6 year period of lunar nodal variation (Foreman 1977, 1978).

Inverse model

The inverse model is a standard application of the Oregon State University Tidal Inversion Software, “OTIS” (Egbert & Erofeeva 2002). Assimilation models simultaneously honour both the assimilated data and a set of dynamical equations, with optimization specified in some least squares sense. One can regard the process as objectively “nudging” a dynamical solution into satisfactory agreement with the data, or using dynamics to interpolate and extrapolate data-based fields to the entire model domain. The mathematical details of data assimilation for tidal models are beyond the scope of the present paper, and the interested reader should see Egbert & Erofeeva (2002) and other references cited therein.

The domain for an assimilation model of the Ross Sea is $63^\circ\text{--}86^\circ\text{S}$ and 150°E to 140°W . Assimilated data consists of T/P radar altimetry north of $\sim 66^\circ\text{S}$ and the 10 tide gauge and gravimeter sites on the RIS (Fig. 1, Table I). In theory, current meter data can also be assimilated, which would greatly improve the distribution of sites over the open Ross Sea (see Fig. 1). In practice, however, the weak semidiurnal currents preclude an acceptable solution in that tidal band, while the diurnal currents are dominated by topographically trapped vorticity waves (TVWs). The TVWs may be sensitive to background factors such as stratification and mean flow along the shelf break (Middleton *et al.* 1987), and so are not well described by tide-only, depth-integrated barotropic models.

Two factors concerning the application of OTIS to this Ross Sea model are worthy of brief mention here. First, we note that the data constraint is strongest in the region north of $\sim 66^\circ\text{S}$ covered by T/P altimetry. In order to allow the least squares solution to be biased towards the 10 RIS tide gauges while still attempting to fit the T/P data, *a priori* errors for the T/P data are assumed to be larger (3–11 cm) than those for the RIS tide gauges (0.5 cm). To account for errors in dynamical equations, the local model data misfit is scaled by the inverse of the prior error covariance map, which in turn depends on the amplitude of the tides in the prior model solution. Since the largest tidal amplitudes are found in the southern Ross Sea, the largest errors in the dynamical equations are assumed there. The combination of assumed low error in data and large error in dynamics biases the fit for the RIS towards data. Second, we use a 200 km

Table III. Periods of the ten tidal harmonics included in the CATS forward models, and critical latitude (ψ_{crit}) for semidiurnal tides. Only M_2 , S_2 , N_2 , K_1 , O_1 and P_1 are included explicitly in the data assimilation. For the inverse models, K_2 , Q_1 , M_f and M_m are taken from CATS02.01.

Harmonic	M_2	S_2	N_2	K_2	K_1	O_1	P_1	Q_1	M_f	M_m
Period (h)	12.42	12.00	12.66	11.97	23.93	25.82	24.07	26.87	327.9	661.3
ψ_{crit}	74.47°	85.76°	70.98°	90.0°						

Table IV. Comparison of the overall performance of models for tide heights on the Ross Ice Shelf, for the four most energetic harmonics (M_2 , S_2 , K_1 and O_1). The value shown for each model and harmonic is the root-mean-square (RMS) difference (cm) between the modelled and observed sine wave for the specified harmonic frequency, thus taking into account both amplitude and phase errors. Inverse solutions (RS02.01_ σ_ϵ) are ordered by increasing fit to data (decreasing σ_ϵ).

Model	Tidal harmonic			
	M_2	S_2	K_1	O_1
MacAyeal (1984)	12.0	6.9	12.7	5.1
CATS01.02	3.5	7.2	10.0	5.6
CATS02.01	3.1	5.3	8.9	5.2
RS02.01_3.0	4.4	7.3	3.5	4.1
RS02.01_1.0	3.9	5.3	3.1	3.7
RS02.01_0.3	2.8	3.0	2.6	3.2
RS02.01_0.1	2.0	1.7	2.2	2.8

interior decorrelation length scale in order to maintain smoothness of the inverse solution with respect to the assimilated tidal height records from the RIS. This value is chosen in OTIS depending on the resolution of the model domain, and the 200 km value corresponds to about 20 grid cells in each direction. Note that, since Williams & Robinson (1980) and M84 tabulated the amplitude and phase coefficients for only six tidal harmonics, only these tides are included in the data assimilation model. For the remaining four tidal harmonics we use the fields from the optimum forward model CATS02.01.

The designations for the present set of Ross Sea assimilation models are {RS02.01_ σ_ϵ : $\sigma_\epsilon=0.1, 0.3, 1.0, 3.0$ }, where σ_ϵ is the “damping” parameter and $\sigma_\epsilon=1$ implies that our *a priori* estimates of dynamical and data errors were correct. Changing this parameter in a range around unity allows us to test these error assumptions. In general we choose σ_ϵ such that data have the necessary effect on constraining the SSH solutions, but without introducing unrealistic spatial structure in either the velocity fields or the dynamic residual (the numerical “forcing” required to nudge the prior model to the final inverse solution). For the present study, $\sigma_\epsilon=0.1$ and 0.3 are both acceptable models.

The model bathymetric grid

The bathymetric grid is based on ETOPO-5 (National Geophysical Data Center, 1986), but significantly updated as described in Padman *et al.* (2002). Additional modifications have been made to the Filchner and Ronne ice shelves following analyses of ERS radar altimetry (Fricker & Padman 2002). For the open Ross Sea, we obtained data from the National Geophysical Data Center and, after quality control, regrided and interpolated these data to the CATS grid. The resultant map of water depth for the open water section of the Ross Sea is very similar to that presented by Brancolini *et al.* (1995). For the ocean cavities under the RIS (and other major ice shelves), water depth is

replaced with water column thickness. For simplicity, we refer to this value as “depth” for the remainder of this paper. The depth values for the RIS were kindly provided by D. Holland (personal communication 1999) based on the measurements by Greishar & Bentley (1980). The RIS cavity geometry has been further updated by changing the grounding line to match the 1993 SCAR coastline (Scientific Committee for Antarctic Research 1993). For CATS02.01 and the inverse model, additional modifications have been made along the Siple Coast grounding line following Gray *et al.* (2002).

Model evaluation

Tide heights

The principal test of performance is the model fit to the measured tidal complex amplitudes (generally expressed as amplitude and Greenwich phase lag) for the 10 tidal measurement sites on the RIS (Table I). Table IV summarizes these results for the M84 model, CATS01.02 (quadratic friction), CATS02.01 (linear friction), and the set of data assimilation models {RS02.01_ σ_ϵ : $\sigma_\epsilon=0.1, 0.3, 1.0, \text{ and } 3.0$ }. As a measure of goodness of fit for each tidal harmonic for each model, we use the root-mean-square (RMS) difference between the modelled and observed sine wave for the specified harmonic frequency. This measure thus takes into account both amplitude and phase differences. The improvement from M84 to CATS01.02 is quite small, with the notable exception of M_2 . It is difficult to understand the anomalous improvement in M_2 and we hypothesize that there may have been numerical reasons, possibly related to the presence of the M_2 critical latitude ($\sim 74.5^\circ\text{S}$) in the model domain, why the M84 model performed so poorly at predicting this harmonic.

The linear friction model, CATS02.01, performs better than CATS01.02 with quadratic friction. Linear-friction models dissipate a greater fraction of the total tidal energy loss in deep water where the currents are relatively small. For the linear drag coefficient that was used ($R = 0.003$), CATS02.01 also predicts more total dissipation within the model domain than CATS01.02 does. This result hints that the standard dynamical model (CATS01.02) may miss significant tidal energy loss terms such as baroclinic tide generation, interactions between the ocean and both sea ice and ice shelves, and scattering and other dissipative processes associated with energetic diurnal TVWs along the shelf break.

Inverse models assimilate the 10 ice shelf tide records in the model solution; therefore the comparison between these models and data in Table I is not a true test of model skill. Instead, the tests indicate the level of fit that can be achieved with a specific choice of σ_ϵ . As expected, the most strongly data-constrained model, RS02.01_0.1, has the lowest RMS errors. At the other end of this scale,

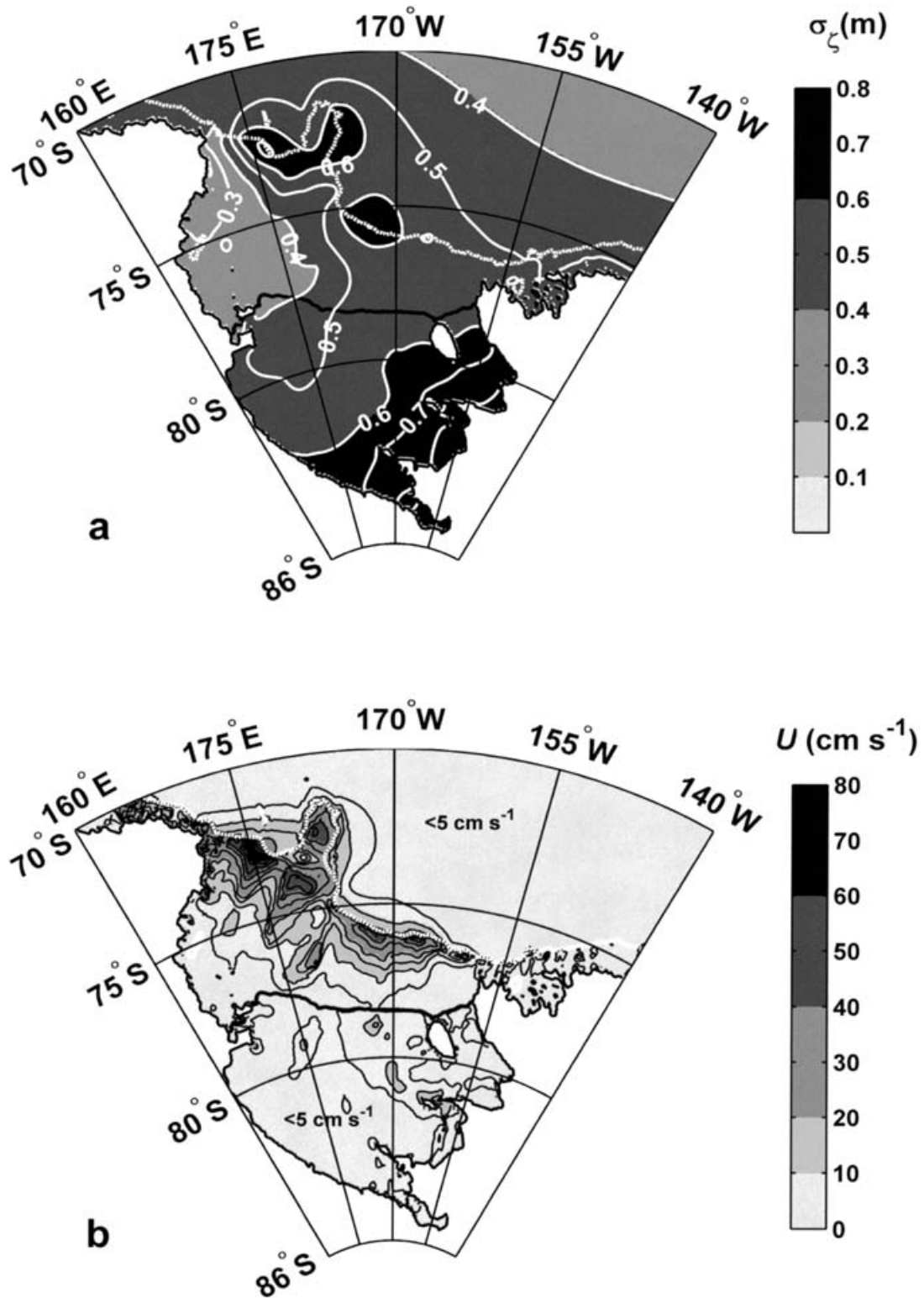


Fig. 2. a. Standard deviation of tide height, σ_ζ (m), using the RS02.01_0.1 inverse solution for six tidal harmonics and CATS02.01 for the remaining four minor harmonics. Shading interval is 0.2 m; contour interval (white lines) is 0.1 m. Values of σ_ζ exceed 0.8 m along the Siple Coast. For geographical reference, the ice front (solid black line) and 1000 m isobath (dashed white line) are shown. **b.** Mean current speed, U (cm s^{-1}), based on the 10-component CATS02.01 forward model. Shading interval is 10 cm s^{-1} below 20 cm s^{-1} , then 20 cm s^{-1} thereafter. Contour interval (black lines) is 5 cm s^{-1} below 20 cm s^{-1} , then 10 cm s^{-1} thereafter. Values exceed 70 cm s^{-1} along the north-western shelf break. Values of 2–20 cm s^{-1} are found over the central Ross Sea continental shelf, and values of 2–8 cm s^{-1} are common under the RIS. The maximum current speed at spring tide is typically 2–3 times greater than U .

Table V. Comparison of tide height harmonic coefficients on the Ross Ice Shelf (RIS), for measured values (Meas.) and three models, CATS01.02 (#1), CATS02.01 (#2), and RS_02.01_0.1 (#3). Stations are ordered as in Table I, roughly clockwise around the perimeter of the RIS from the eastern end of the ice front (LAS) to the western end (McMurdo). For each station we show measured amplitude (a , cm), difference between modelled and measured amplitude (Δa , cm), measured phase (p , $^\circ$), and difference between modelled and measured phase (Δp , $^\circ$). The root-mean-square (RMS) errors (cm) in the last line take into account both amplitude and phase differences.

		M_2				S_2				K_1				O_1			
		Meas.	#1	#2	#3	Meas.	#1	#2	#3	Meas.	#1	#2	#3	Meas.	#1	#2	#3
LAS	$a, \Delta a$	3	+2	+2	+1	5	+4	+4	0	34	+6	+6	+2	25	+8	+8	+4
	$p, \Delta p$	35	+11	+24	+24	342	-10	+6	-3	154	-11	-10	0	141	-7	-8	-4
C36	$a, \Delta a$	8	-4	-3	-5	6	+2	+2	-1	37	+7	+7	+1	32	+3	+4	+1
	$p, \Delta p$	75	+7	+21	+21	25	-12	+8	+3	160	-3	-1	+4	153	-5	-6	0
RI	$a, \Delta a$	5	+4	+4	+1	10	+7	+7	-1	44	+3	+4	-3	38	0	0	-4
	$p, \Delta p$	130	-45	-28	-26	26	-11	+11	+2	160	-14	-8	-1	140	-1	+1	+2
Base	$a, \Delta a$	8	+2	+1	0	10	+9	+6	0	43	+7	+10	-2	35	+5	+6	+1
	$p, \Delta p$	213	-39	-28	-22	112	0	+15	-2	186	-14	-5	+1	174	-10	-6	-3
J9	$a, \Delta a$	7	+1	0	0	8	+7	+5	0	37	+11	+13	+2	37	+2	+3	-2
	$p, \Delta p$	205	-29	-21	-14	106	+8	+20	0	191	-18	-10	-4	172	-8	-4	0
F9	$a, \Delta a$	8	+5	+1	+2	11	+18	+5	+1	41	+13	+15	+2	40	+2	+3	0
	$p, \Delta p$	258	-7	+1	-2	142	+59	+72	+14	206	-15	-5	-2	190	-8	-3	-1
C16	$a, \Delta a$	3	-1	-2	-1	2	+3	-1	0	31	+7	+8	+1	27	+4	+5	+3
	$p, \Delta p$	310	-15	-24	-3	160	+87	+82	-9	200	-8	-1	+1	190	-8	-5	0
O19	$a, \Delta a$	4	0	-2	-1	2	+5	+1	0	31	+7	+7	-1	29	+2	+2	+1
	$p, \Delta p$	340	-2	+14	+5	190	+93	+110	+10	208	-6	0	+1	196	-5	-4	+1
C13	$a, \Delta a$	3	0	-1	0	4	+2	-1	-3	30	+5	+5	0	34	-5	-5	-4
	$p, \Delta p$	300	+57	+81	+60	130	+171	-160	+90	200	-4	+1	0	190	-6	-5	+1
McMurdo	$a, \Delta a$	4	+1	0	+1	2	+7	+4	0	26	+3	+2	0	26	-2	-2	-1
	$p, \Delta p$	6	+11	+24	+15	268	+59	+75	+64	196	+6	+11	-1	186	+4	+5	+2
RMS error		-	4	3	2	-	10	7	2	-	11	10	2	-	6	5	3

RS02.01_3.0 does not improve the fit for M_2 and S_2 relative to the CATS models, although K_1 and O_1 are improved. From other considerations, we consider RS02.01_0.1 to be the optimum inverse model for this region.

Harmonic amplitude and phase values for the 10 RIS tidal records are listed in Table V, along with the corresponding values from CATS01.02, CATS02.01, and RS02.01_0.1. Some differences between data and models may be due to errors in the harmonics derived from the tidal records: with the exception of McMurdo, all records are < 2 months duration and of uncertain quality (the original gravimetry data are not available to us for reanalysis). The M_2 and O_1 tides are reasonably well represented by the forward models throughout the RIS cavity, although both models routinely over predict O_1 amplitude on the eastern side of the RIS. Forward-model errors in S_2 are also largest in this region. The improvement from CATS01.02 to CATS02.01 at the southernmost station F9 is largely due to the revision of the grounding line following Gray *et al.* (2002). We note, however, that S_2 amplitude is too high at LAS, where the tidal energy first enters the RIS cavity, and at the high-quality McMurdo station, also near the ice front. This result suggests that too much S_2 energy is present even north of the ice front, which in turn may indicate errors in the T/P-based open boundary conditions at 58°S . It is possible that uncorrected radiational tides (ocean response to air pressure variations) in the T/P data contaminate the boundary conditions for our models. The modelled K_1 tide is routinely higher than the measured values, including at the LAS and

McMurdo ice front stations. The most likely cause of diurnal-band errors in our forward models is the contribution of TVWs to the total tidal energy flux: mistakes in the production and dissipation rates of diurnal energy along the continental shelf break will affect tidal predictions everywhere that this energy propagates.

The variability of tide heights throughout the Ross Sea is shown by the standard deviation of the tide height obtained from the inverse model RS02.01_0.1 (Fig. 2a). This value, denoted $\sigma_\zeta(x, y)$, is given by

$$\sigma_\zeta(x, y) = \left(\sum_{i=1}^{i=10} a_i^2(x, y) \right)^{1/2}$$

where a_i is the amplitude of the i 'th tidal harmonic. Since RS02.01_0.1 only produces inverse solutions for the six most energetic tidal harmonics, the other four (see Table III) are taken from CATS02.01. The value of σ_ζ ranges from < 0.3 m along the Victoria Land coast to > 0.8 m along the Shirase and Siple coasts. The maximum tide height magnitude is typically 2–2.5 times σ_ζ , and maximum spring tidal range is $\sim 4\sigma_\zeta$, so daily changes of > 3 m are possible along the Siple Coast.

As an independent test of the performance of RS02.01_0.1 relative to the forward models, Fig. 3 compares modelled and measured values of the height change δh obtained along the southern Siple Coast with InSAR (see next section). The mean absolute errors for CATS01.02, CATS02.01, and RS02.01_0.1 are 34, 22, and

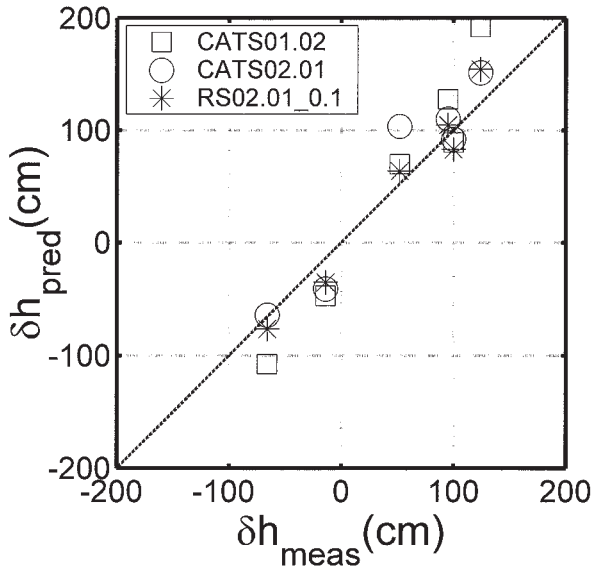


Fig. 3. Comparison of InSAR-derived height differences (δh_{meas}) with the predicted values (δh_{pred}) of three tidal models, CATS01.02 (\square), CATS02.01 (\circ), and RS02.01_0.1 ($*$).

17 cm, respectively. A major potential source of error arises from the inverse barometer effect (IBE; Rignot *et al.* 2000). The IBE is a depression of ocean and freely floating ice surface elevation of ~ 1 cm for each 1 millibar increase in atmospheric pressure. We do not have the atmospheric pressure data necessary to make this correction to tide predictions of δh . A typical expression of the IBE in δh from SAR interferometry is, however, ~ 10 – 20 cm (Rignot *et al.* 2000): thus, values of the mean absolute error less than ~ 20 cm can be regarded as being as accurate as possible when the IBE correction cannot be made. Both CATS02.01 and RS02.01_0.1 are close to this limit.

As a cautionary comment, we note that modelling sensitivity studies (not shown here) demonstrate that tide heights under the RIS are very sensitive to uncertainties in water column thickness and grounding line location. The Siple Coast side of the RIS is known to have shallow water column thicknesses compared with the deeper western side. Thus, relatively minor changes in the thickness of ice discharged from the Siple Coast ice streams to the RIS may have significantly altered the cavity geometry, and thus also the tides, between the epochs of gravimeter data collection in the 1970s and the more recent acquisition of InSAR data. That is, a tidal model constrained to this set of gravimeter data may not be the optimum model for comparison with δh from InSAR measurements obtained during the more recent epoch.

Tidal currents

Predicting tidal currents is much more difficult than predicting SSH. In the Antarctic, two factors that contribute

to this difficulty are the presence of diurnal TVWs along the shelf break, and the anomalous behavior of currents near a tidal constituent's critical latitude. We discuss diurnal TVWs in more detail in the following paragraphs. The critical latitude for tidal constituent 'X', $\psi_{\text{crit}}(X)$, is the latitude at which the tidal frequency $\omega(X)$ equals the Coriolis frequency, f . The values for M_2 and S_2 are $\sim 74.47^\circ$ and $\sim 85.76^\circ$, respectively (see Table III). The vertical structure of tidal currents near ψ_{crit} can become quite complex (Robertson *et al.* 2001, Robertson 2001a, 2001b, Makinson 2002), making it difficult to compare currents from depth-averaged models with measured currents at specific depths. In the Ross Sea, however, semidiurnal tides are generally weak.

The strongest tidal currents so far recorded in the Ross Sea were measured on the continental shelf near the shelf break east of Cape Adare in the north-west Ross Sea (J Mooring C, Jaeger *et al.* 1996, see Table II). Currents at this site frequently exceed 40 cm s^{-1} at spring tide, with the energy being associated primarily with K_1 and O_1 diurnal TVWs. The model that most accurately represents the current speed distribution at this mooring is CATS02.01, the forward model with linear friction. The inverse model RS02.01_0.1 performs less well than CATS02.01 here because there are no assimilated height data in this region, which is well south of the T/P orbit and well north of the ice shelf gravimetry records. However, even CATS02.01 performs poorly at predicting the phase of tidal currents along the shelf break. Diurnal TVWs are sensitive to small-scale bathymetric variability, stratification, and mean flow, and so are poorly represented in depth-integrated, tide-only models with significant uncertainties in the bathymetry (Robertson *et al.* 1998, Padman & Kottmeier 2000). Increased model sophistication and, in particular, more detailed bathymetry data, will be required to improve predictions of tidal velocity at a specified place and time.

For many oceanic applications, however, it is sufficient to adequately predict the typical magnitude of tidal currents without worrying about phase. The time-averaged mean modelled current speed,

$$U(x,y) = \langle (u(x,y,t)^2 + v(x,y,t)^2)^{1/2} \rangle$$

where angle brackets denote time averaging at a grid node at location (x, y) , is a useful guide to spatial distribution of tidal currents. For each node we calculate U as the average of 180 days of modelled currents. The dominant feature of $U(x, y)$ in CATS02.01 is the ridge of $U > 20 \text{ cm s}^{-1}$ along the north-western shelf break (Fig. 2b). Peak values of U exceed 70 cm s^{-1} . The maximum modelled current speed at each location is typically 2–3 times greater than U , suggesting that spring tidal currents may exceed 1.5 m s^{-1} along some sections of the shelf break. Over the continental shelf, U occasionally exceeds 20 cm s^{-1} over the main banks (Crary, Mawson, Pennell, and Ross) of the north-western Ross Sea. The tidal currents in these areas are mainly due to

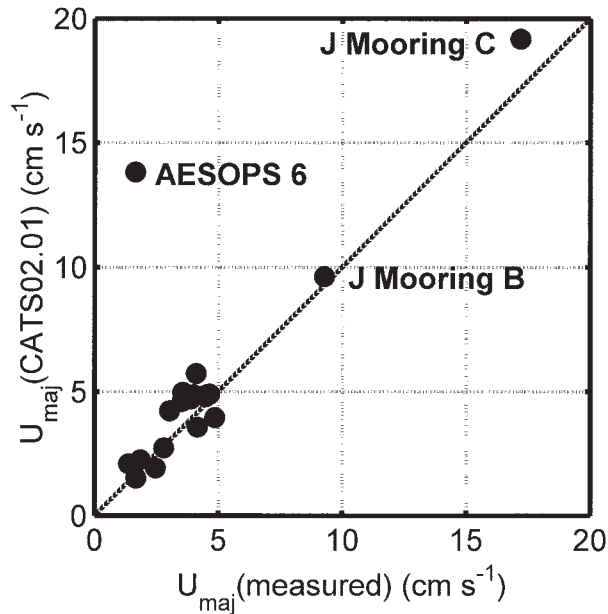


Fig. 4. Comparison of major axis of K_1 tidal ellipse, measured at selected current meter locations (see Fig. 1 and Table II), U_{maj} (measured), with modelled value from the CATS02.01 forward model (U_{maj} (CATS02.01)). The dashed diagonal line indicates equivalence. The uncertainty in each estimate of U_{maj} (measured) is $\sim 1\text{--}2\text{ cm s}^{-1}$, due to instrument noise and analysis limitations on these data.

diurnal TVW energy that has leaked southward from the shelf break along the edges of the banks. One corollary to this view of tidal kinetic energy flux is that tidal currents over the central continental shelf are not easily predicted: the phases of the diurnal TVWs along the banks will depend on the phases of the TVWs along the shelf break, and the latter are sensitive to stratification changes (Cummins *et al.* 2000) and mean flow variability (Foldvik *et al.* 1990) at the shelf break and upper continental slope. It is likely that significant features of the density structure, such as the overflowing plumes of dense High Salinity Shelf Water (Whitworth *et al.* 1998) and seasonally varying upper ocean stratification, change energy level and phase of TVWs at the shelf-break, and so ultimately also modify mid-shelf currents. Significant semidiurnal energy is frequently seen in ice drift and upper ocean ADCP records, but is due to wind forcing of near-inertial oscillations rather than tides.

Over the continental shelf and slope north of the RIS front, modelled annual averaged thermohaline and wind-forced currents in both the surface and deep layers are typically $2\text{--}8\text{ cm s}^{-1}$ (Assmann *et al.* 2003, fig. 3). The strongest currents are along the shelf break and slope of the north-west Ross Sea, where tidal currents are also strong, and along the RIS front. In most areas, the mean tidal current is much larger than the mean non-tidal flow, indicating that the tidal contribution to benthic stirring and

the associated increased in the effective benthic friction coefficient (Robertson *et al.* 1998), and dynamic effects on the sea ice (Padman & Kottmeier 2000), will be significant.

Mean tidal currents under the RIS are generally less than 10 cm s^{-1} , with the exception of some regions of very shallow water along the Siple Coast. In comparison, mean currents under the Filchner–Ronne Ice Shelf in the southern Weddell Sea can exceed 50 cm s^{-1} near the Ronne Ice Front (Robertson *et al.* 1998, plate 3b). The fundamental differences between the tides in the Weddell and Ross Seas are that global ocean semidiurnal tides are much stronger near the Weddell than near the Ross Sea, and both basin geometries are more favourable to resonance of the semidiurnal than of the diurnal tides. Even though the currents under the RIS are relatively weak, tides are still the largest single source of kinetic energy and turbulence there since the cavity is insulated from direct surface forcing (M84). Typical mean flows associated with thermohaline forcing within the RIS cavity are only $\sim 1\text{ cm s}^{-1}$ (Holland *et al.* 2003, fig. 8).

Significant errors within the numerical models are best identified through comparisons of modelled and measured amplitude and phase for specific harmonics rather than through statistical quantities such as $U(x, y)$. We noted above that, for a variety of reasons, phase for diurnal current components is difficult to model. However, our ability to predict U reasonably well at J Mooring C suggests that the major axes of current ellipses might be more easily predictable. Since the diurnal K_1 harmonic is the most energetic tide in the Ross Sea, we compare the major axis of the K_1 tidal ellipse ($U_{\text{maj}}(K_1)$) at the current meter locations shown in Fig. 1 with predictions from CATS02.01 (Fig. 4). The mean absolute error for this comparison is $\sim 1.4\text{ cm s}^{-1}$, and a similar result is found for O_1 . The largest values of $U_{\text{maj}}(K_1)$ and $U_{\text{maj}}(O_1)$ are found at the previously discussed J Mooring C (Table II). These values are slightly overestimated by CATS02.01. The largest errors in $U_{\text{maj}}(K_1)$ and $U_{\text{maj}}(O_1)$ occur for the current meter located between Mawson and Pennell banks in the north-western Ross Sea (site AESOPS 06, see Table II). While the measured value of $U_{\text{maj}}(K_1)$ is only $\sim 2\text{ cm s}^{-1}$, CATS02.01 predicts a value of $\sim 14\text{ cm s}^{-1}$. We do not understand this discrepancy at present, but suspect that it indicates a more rapid attenuation of the diurnal TVWs than is accounted for in CATS02.01, or destructive interference of TVWs following multiple paths around the bank/trough structures including the nearby “promontory” formed by Iselin Bank. Phase errors associated with ignoring TVW response to stratification and mean flow in our models may shift the modelled regions of constructive and destructive interference relative to their true locations. No attempt is made here to validate the models’ performance with respect to tidal current phase, for reasons that have been discussed above.

With the exception of J Mooring C, $U_{\text{maj}}(M_2)$ and $U_{\text{maj}}(S_2)$ never exceed $\sim 1.5\text{ cm s}^{-1}$. The measured value of $U_{\text{maj}}(M_2)$

at J Mooring C is $\sim 7 \text{ cm s}^{-1}$, but this large value is not seen in any of our models. We hypothesize that this value arises through critical latitude effects as the barotropic M_2 tide flows over the nearby continental slope (Robertson *et al.* 2003).

Discussion and conclusion

We can now predict variability of ice shelf surface height with an RMS accuracy of $\sim 10\text{--}20 \text{ cm}$ using the new tidal models discussed in this paper. Taking the M84 model as the previous benchmark, the most important factors in improved model performance are: SAR-based updating of the RIS grounding line; updated open-ocean boundary conditions using a global model that is consistent with TOPEX/Poseidon radar altimetry; and formal assimilation of gravimeter and tide gauge data from the RIS. We have also shown that the skill of the dynamics-based models can be improved by modifying the dissipation mechanisms for tidal energy, notably the representation of bottom friction. Somewhat surprisingly, linear friction performs much better than quadratic friction. Further significant improvements will require new height data, which may be obtained from gravimeters or GPS units on the ice shelves, tide gauges on the seabed, or satellite altimetry. Of those, altimetry is the most likely to provide sufficient coverage over a wide area in the foreseeable future (see Fricker & Padman 2002).

In contrast to the satisfactory prediction of tidal heights, we are still not able to make an accurate prediction of the tidal current velocity at a specific location and time, especially near the shelf break. The new models do, however, improve the accuracy of bulk statistical properties such as mean tidal current speed. Very strong currents, sometimes exceeding 1 m s^{-1} at spring tide, are predicted in a narrow band along the continental shelf break and upper slope of the north-western Ross Sea. Since this is a region where dense shelf water first enters the deep ocean to provide the Ross Sea contribution to Antarctic Bottom Water (Gordon 1975, Orsi *et al.* 1999), understanding the tide's role in mixing the dense water plume with the ambient water is a priority for further research. Tide height data from near the shelf break is required to help constrain the barotropic tidal solution for diurnal harmonics in this region. The Ross Sea shelf break is well south of the T/P orbit and is too frequently covered with sea ice to allow for collection of high-quality satellite altimetry. We therefore advocate the collection of bottom pressure data in any programs operating near the shelf break. We can further improve tidal current prediction through assimilation of current meter data and by baroclinic modelling of the energetic diurnal tides. The latter effort would assess the sensitivity of diurnal TVWs to stratification, mean flow, and the small-scale topographic roughness that is presently inadequately characterized because of the paucity of bathymetric data. Many of these proposed activities will

take place within the “AnSlope” (Antarctic Slope) program to be carried out near the north-west Ross Sea shelf break in 2003/04.

Satellite altimetry may offer the best hope for improved tidal models of the Ross Sea. Fricker & Padman (2002) showed that ERS radar altimetry over the Filchner–Ronne Ice Shelf (FRIS) in the Weddell Sea could provide reasonable estimates of tide height fields north of the ERS turning latitude of $\sim 81.5^\circ\text{S}$. In a future study we will explore a similar application of ERS altimetry to the RIS. Unfortunately, much of the RIS is south of 81.5°S , and the tides under the RIS are smaller than those of the FRIS so that the quality of ERS-derived tides may not improve upon the existing numerical models. However, the Geoscience Laser Altimeter System (GLAS), to be launched on ICESat in late 2002, should provide much more accurate tidal fields over the entire floating portion of the Antarctic ice sheet. At the end of its 3-year intended mission life, it should be possible to derive very accurate tidal height fields for this region.

Acknowledgements

We appreciate the constructive comments of two anonymous reviewers and the efforts of our associate editor, Stan Jacobs. We thank Doug MacAyeal for stimulating our interest in the tides of the Ross Sea. This work was supported by NASA (NAG5-7790) and the National Science Foundation (OPP-9896006 and OCE-9906926).

References

- ASSMANN, K., HELLMER, H.H. & BECKMANN, A. 2003. Seasonal variation in circulation and watermass distribution on the Ross Sea continental shelf. *Antarctic Science*, **15**, xxx–xxx.
- BRANCOLINI, G., BUSETTI, M., MARCHETTI, A., DE SANTIS, L., ZANOLLA, C., COOPER, A.K., COCHRANE, G.R., ZAYATZ, I., BELYAEV, V., KNYAZEV, M., VINNIKOVSKAYA, O., DAVEY, F.J. & HINZ, K. 1995. Descriptive text for the seismic stratigraphic atlas of the Ross Sea, Antarctica. *Antarctic Research Series*, **68**, A271–A286.
- CUMMINS, P.F., MASSON, D. & FOREMAN, M.G.G. 2000. Stratification and mean flow effects on diurnal tidal currents off Vancouver Island. *Journal of Physical Oceanography*, **30**, 15–30.
- EGBERT, G.D. 1997. Tidal data inversion: Interpolation and inference. *Progress in Oceanography*, **40**, 53–80.
- EGBERT, G.D. & EROFEEVA, S. 2002. Efficient inverse modelling of barotropic ocean tides. *Journal of Atmospheric and Oceanic Technology*, **19**, 183–204.
- FOLDVIK, A., MIDDLETON, J.H. & FOSTER, T.D. 1990. The tides of the southern Weddell Sea. *Deep-Sea Research*, **37**, 1345–1362.
- FOREMAN, M.G.G. 1977. *Manual for tidal heights analysis and prediction*. Pacific Marine Science Report 77–10. Sidney, BC: Institute of Ocean Sciences, Patricia Bay, 97 pp.
- FOREMAN, M.G.G. 1978. *Manual for tidal currents analysis and prediction*. Pacific Marine Science Report 78–6. Sidney, BC: Institute of Ocean Sciences, Patricia Bay, 70 pp.
- FRICKER, H.A. & PADMAN, L. 2002. Tides on Filchner–Ronne Ice Shelf from ERS radar altimetry. *Geophysical Research Letters*, **29**, 10.1029/2001GL014175.

- GORDON, A.L. 1975. An Antarctic oceanographic section along 170°E. *Deep-Sea Research*, **22**, 357–377.
- GRAY, L., SHORT, N., BINDSCHADLER, B., JOUGHIN, I., PADMAN, L., VORNBERGER, P. & KHANANIAN, A. 2002. RADARSAT interferometry for Antarctic grounding zone mapping. *Annals of Glaciology*, **34**, 269–276.
- GREISCHAR, L.L. & BENTLEY, C.R. 1980. Isostatic equilibrium grounding line between the West Antarctic inland ice sheet and the Ross Ice Shelf. *Nature*, **283**, 651–654.
- HOLLAND, D.M., JACOBS, S.S. & JENKINS, A. 2003. Modelling the ocean circulation beneath the Ross Ice Shelf. *Antarctic Science*, **15**, xxx–xxx.
- JAEGER, J.M., NITTRouer, C.A., DEMASTER, D.J., KELCHNER, C. & DUNBAR, R.B. 1996. Lateral transport of settling particles in the Ross Sea and implications for the fate of biogenic material. *Journal of Geophysical Research*, **101**, 18 479–18 488.
- LEFÈVRE, F., LYARD, F.H., LE PROVOST, C. & SCHRAMA, E.J.O. 2002. FES99: a global tide finite element solution assimilating tide gauge and altimetric information. *Journal of Atmospheric and Oceanic Technology*, **19**, 1345–1356.
- LE PROVOST, C., LYARD, F., MOLINES, J.M., GENCO, M.L. & RABILLOU, F. 1998. A hydrodynamic ocean tide model improved by assimilating a satellite altimeter-derived data set. *Journal of Geophysical Research*, **103**, 5513–5529.
- MACAYEAL, D.R. 1984. Numerical simulations of the Ross Sea tides. *Journal of Geophysical Research*, **89**, 607–615.
- MAKINSON, K. 2002. Modelling tidal current profiles and vertical mixing beneath Filchner–Ronne Ice Shelf, Antarctica. *Journal of Physical Oceanography*, **32**, 202–215.
- MIDDLETON, J.H., FOSTER, T.D. & FOLDAVIK, A. 1987. Diurnal shelf waves in the southern Weddell Sea. *Journal of Physical Oceanography*, **17**, 784–791.
- NATIONAL GEOPHYSICAL DATA CENTER. 1986. *ETOPO-5 bathymetry/topography data. Data Announcement 88-MGG-02, National Oceanic and Atmospheric Administration*. Boulder, CO: US Department of Commerce.
- ORSI, A.H., JOHNSON, G.C. & BULLISTER, J.L. 1999. Circulation, mixing, and production of Antarctic Bottom Water. *Progress in Oceanography*, **43**, 55–109.
- PADMAN, L. & KOTTMEIER, C. 2000. High-frequency ice motion and divergence in the Weddell Sea. *Journal of Geophysical Research*, **105**, 3379–3400.
- PADMAN, L., FRICKER, H.A., COLEMAN, R., HOWARD, S. & EROFEEVA, S. 2002. A new tidal model for the Antarctic ice shelves and seas. *Annals of Glaciology*, **34**, 247–254.
- PAWLOWICZ, R., BEARDSLEY, B. & LENTZ, S. 2002. Classical tidal harmonic analysis including error estimates in MATLAB using T_TIDE. *Computers and Geosciences*, in press.
- PILLSBURY, R.D. & JACOBS, S.S. 1985. Preliminary observations from long-term current meter moorings near the Ross Ice Shelf, Antarctica. *Antarctic Research Series*, **43**, 87–107.
- RIGNOT, E., PADMAN, L., MACAYEAL, D.R. & SCHMELTZ, M. 2000. Observation of ocean tides below the Filchner and Ronne Ice shelves, Antarctica, using synthetic aperture radar: comparison with tide model predictions. *Journal of Geophysical Research*, **105**, 19 615–19 630.
- ROBERTSON, R. 2001a. Internal tides and baroclinicity in the southern Weddell Sea. 1. Model description. *Journal of Geophysical Research*, **106**, 27 001–27 016.
- ROBERTSON, R. 2001b. Internal tides and baroclinicity in the southern Weddell Sea, 2, Effects of the critical latitude and stratification. *Journal of Geophysical Research*, **106**, 27 017–27 034.
- ROBERTSON, R., BECKMANN, A. & HELLMER, H. 2003. Tidal dynamics in the Ross Sea. *Antarctic Science*, **15**, xxx–xxx.
- ROBERTSON, R., PADMAN, L. & EGBERT, G.D. 1998. Tides in the Weddell Sea. *Antarctic Research Series*, **75**, 341–369.
- ROBERTSON, R.A., PADMAN, L. & LEVINE, M.D. 2001. A correction to the baroclinic pressure gradient term in the Princeton Ocean Model. *Journal of Atmospheric and Oceanic Technology*, **18**, 1068–1075.
- SCIENTIFIC COMMITTEE FOR ANTARCTIC RESEARCH. 1993. *Antarctic Digital Database on CD-ROM*. Cambridge, UK: Scott Polar Research Institute.
- WHITWORTH III, T., ORSI, A.H., KIM, S.-J. & NOWLIN JR, W.D. 1998. Water masses and mixing near the Antarctic Slope Front. *Antarctic Research Series*, **75**, 1–27.
- WILLIAMS, R.T. & ROBINSON, E.S. 1980. The ocean tide in the southern Ross Sea. *Journal of Geophysical Research*, **85**, 6689–6696.